Biophysical Journal, Volume *120*

Supplemental information

Phosphofructokinase relocalizes into subcellular compartments with liquid-like properties in vivo

SoRi Jang, Zhao Xuan, Ross C. Lagoy, Louise M. Jawerth, Ian J. Gonzalez, Milind Singh, Shavanie Prashad, Hee Soo Kim, Avinash Patel, Dirk R. Albrecht, Anthony A. Hyman, and Daniel A. Colón-Ramos

Supplementary Methods

C. elegans strains and transgenic lines

For C-terminal endogenous tagging of PFK-1.1, a cell-specific CRISPR protocol (1, 2) was used to insert two flippase recombinase target (FRT) sites flanking *let-858* 3'-UTR that contains a transcriptional stop motif followed by a GFP sequence in front of the endogenous *pfk-1.1* 3'-UTR in the X chromosome (*pfk-1.1(ola368)*). Upon injection of cell-specific transgenes expressing FLPase, the *let-858* 3'-UTR containing the transcriptional stop motif is excised, leaving GFP fused to the C-terminus of PFK-1.1. To achieve specific expression of PFK-1.1::GFP in neurons and the body wall muscle, *unc-47* and *mig-13* promoters were used to drive the expression of FLPase in those cells.

For generating expression clones, Gateway system (Invitrogen) and Gibson system (New England Biolabs) were primarily used. Transgenic strains (0.5–30 ng/µl) were made using standard techniques (3) and coinjected with markers *Punc-122::gfp, Punc-122::rfp, or Podr-1::rfp*. See Table 1 for all strains used in this study.

Supplementary Table 1. Strains used in this study

Strain Name	Genotype
DCR7312	*olaex4409 [Ppfk-1.1:: pfk-1.1::egfp]*
DCR6732	*pfk-1.1(ola368)[pfk-1.1::FLP-ON::gfp]; olaex4038 [Pmig-13::FLPase]*
DCR6941	*pfk-1.1(ola368)[pfk-1.1::FLP-ON::gfp]; olaex4140 [Punc-47::FLPase]*
DCR6037	*olaex3534 [Punc-47::pfk-1.1::egfp; Punc-47::snb-1::mCherry]*
DCR7155	*olaex4296 [Punc-47::pfk-1.1::mRuby-3; Punc-47::tiar-1a::egfp]*
DCR7151	*olaex4292 [Pttx-3::sl2::pfk-1.1::mRuby-3; Pttx-3::sl2::tiar-1a::egfp]*
DCR3921	*olaex2271 [Punc-47::pfk-1.1::egfp; Punc-47::tom-20::mCherry]*
DCR7799	*olaex4731 [Pttx3::sl2::pfk-1.1::mCh::cry2; Pttx3::sl2::pfk-1.1::egfp]*
DCR7801	*olaex4733 [Pttx3::sl2::mCh::cry2; Pttx3::sl2::pfk-1.1::egfp]*
DCR6426	*olaex3802 [Punc-47::pfk-1.1::egfp; Punc-47::mCherry]*
TV1449	*WyEx505 [Pttx-3::mCherry::erc; Pttx-3::gfp::rab-3]*
DCR1564	*pfk-1.1 (ola72); WyEx505*

DCR6987	*olaex4180 [Pttx-3::gfp::rab-3; Pttx-3::pfk-1.1::mCherry::cry2]; pfk-1.1 (ola72)*
DCR6909	*olaex4123 [Pttx-3::sl2::aldo-1::egfp; Pttx-3::sl2::pfk-1.1::mCh::cry2]*
DCR6445	*olaex3818 [Punc-47::pfk-1.1::egfp::cry2; Punc-47::snb-1::mCh]*
DCR7122	*olaex4276 [Pttx-3::sl2::aldo-1::egfp]*
DCR7124	*pfk-1.1(tm5741); olaex4276*
DCR4761	*olaIs39 [Pttx-3::sl2::pfk-1.1::egfp; Pttx-3::mCh::rab-3]*
DCR7006	*olaIs39; aldo-1(tm5782)*
DCR6094	*olaex3582 [Punc-47::aldo-1::egfp; Punc-47::pfk-1.1::mRuby-3]*

Hybrid microfluidic-hydrogel device set-up and calibration

A reusable microfluidic PDMS device was fabricated to deliver gases through a channel adjacent to immobilized animals, following protocols as previously described (4). A 50 µm, oxygen-permeable PDMS membrane was permanently bonded using air plasma to create an enclosed arena for gas flow, while the opposite side of the device was permanently bonded to a glass slide for structural integrity. Right-angle inlet and outlet holes were punched in the PDMS for ease of use with high-magnification inverted and upright microscopes. This reusable assembly was cleaned before each use by wiping the PDMS surface with ethanol, drying, and removing any remaining dust with tape. Animals were kept stationary during high-resolution imaging and exposure to shifting gas concentrations at the membrane surface by hydrogel immobilization (5). To prepare the hydrogel assembly, a small volume (2 µL) of gel (20% PEGDA and 0.05% Irgacure 2959 in water) was pipetted onto the center of a hydrophobic glass slide containing a 100 µm thick PDMS spacer with a 6 mm diameter hole in the center, forming a rounded gel droplet. Glass slides or coverslips were rendered hydrophobic by 1 hour exposure to (tridecafluoro-1,1,2,2-tetrahydrooctyl) trichlorosilane vapor in a vacuum chamber, or “gel-adhesive” by 3 min exposure to 5% 3-(trimethoxysilyl)propyl methacrylate in ethanol (5), which covalently grafts methacrylate groups to the glass that in turn covalently bind to the PEG chains of the hydrogel. Animals were then transferred into the solution and a gel-adhesive coverslip was placed over the hydrogel drop supported by the spacer. The assembly was

placed over a UV light source (UVP, model UVGL-15, 4W) and illuminated for 2 minutes at 365 nm for gelation. The coverslip with spacer was carefully lifted off of the hydrophobic slide and a 2 µL drop of muscimol (50 mM in water) was then pipetted directly over the hydrogel disk. The gas device was carefully centered and lowered on top of the hydrogel assembly and clamped into a P2 series holder (Warner Instruments) to complete the closed system. Lastly, microfluidic tubing and components were connected to a nitrogen tank set to approximately 1-10 psi using a low-pressure regulator. To generate hypoxic conditions in the hydrogel, nitrogen flow was delivered continuously through the device assembly and confirmed by observing bubbles in a waste beaker filled with water connected with tubing to the device outlet. To generate normoxic conditions in the hydrogel, the nitrogen tank was turned off and the inlet tubing was immediately disconnected at the tank. Note that, in addition to the 0% oxygen condition, we also repeated the hypoxic experiments using 8% oxygen condition in the same setup and obtained similar results (data not shown). *C. elegans* can survive anoxic condition for a whole day (6), and for our hypoxic experiments, which ranged from minutes to an hour, the animals were rescued and shown to be viable post transient hypoxia.

For device calibration, oxygen dynamics within the hydrogel were monitored by adding 4 µL of an oxygen sensitive fluorescent dye solution, 0.75 mM $Ru(phen)_3Cl_2$ dissolved in water, onto a 2 µL hydrogel disk before assembling with the gas device. Also, an oxygen probe (Ocean Optics HIOXY-PI600) was plugged into a second outlet to monitor corresponding oxygen concentration levels in the gas channel. A two-way solenoid pinch valve (NResearch 161P091) and custom Arduino controller were used to switch between constant flows of nitrogen or air (21% oxygen) through the device via separate inlets (Fig. S2 A). After this initial set-up, the oxygen probe was calibrated using a two-point calibration during nitrogen (0% oxygen) and air (21% oxygen) flow. MicroManager software was used to configure camera (2x2 binning and 1 second exposure) and acquisition settings (1 frame per second) for monitoring changes in fluorescence intensity

through a 10X Leica objective (0.4 NA), RFP single-band filter set, detected by a Hammamatsu ORCA-ER mounted on a Leica DMI6000B microscope with EXFO X-Cite 120 Fluorescence Illumination System. A sequence of valve switches and tubing change steps were used to control shifts in oxygen concentration and monitored at 1 sample per second with the probe while synchronously recording changes in $Ru(phen)_3Cl_2$ hydrogel intensity (Fig. S2 B). This sequence was saved as a single TIFF stack file and repeated without disturbing the set-up and field of view for a second calibration trial. Mean fluorescence over the full field-of-view (672 x 512 px) centered on the hydrogel disk was measured for all 1200 frames and synchronized with oxygen concentration measurements from the outlet probe in the gas channel. Normalized fluorescence was calculated by scaling between the minimum fluorescence during steady 21% oxygen and the maximum fluorescence at steady 0% oxygen (as fluorescence scales inversely with oxygen). Slight increases in both minimum and maximum fluorescence of the oxygen sensor in the hydrogel were observed over time, likely due to a slow increase in concentration of the oxygen sensitive dye from evaporation. Scaling was adjusted by a linear interpolation of fluorescence envelope between the 0 – 21% oxygen transitions at minute 1 and near minute 15 (Fig. S2 B). To determine the calibration curve between hydrogel fluorescence and oxygen concentration, normalized fluorescence values were plotted against gas channel oxygen measurements, excluding data at times just following valve switches where hydrogel and gas channel concentrations would not be equal due to oxygen diffusion delays. The median fluorescence at binned oxygen concentration values (0.5% O_2 bins) revealed a non-linear relationship between measured oxygen percent and fluorescence in the hydrogel (Fig. S2 C). This calibration curve was used to estimate oxygen concentration in the hydrogel based on linear interpolation between binned values (Fig. S2 D). From this, we estimate that switching between 21% and 0% oxygen in the hydrogel requires about 30 seconds to 1 minute, while switching between 0% and 21% oxygen in the hydrogel is nearly immediate. The directional difference in switching dynamics is likely due to the high oxygen concentration in PDMS (with

high gas permeability) from ambient air, making it faster to increase oxygen, although hysteresis in dye fluorescence or kinetics could also contribute. All analysis was completed using MATLAB R2017a.

Microscopy and image processing

Images of fluorescently tagged fusion proteins were captured live in *C. elegans* nematodes using a 60 CFI Plan Apo VC, numerical aperture 1.4, oil-immersion objective on an UltraView VoX spinning-disc confocal microscope (PerkinElmer Life and Analytical Sciences). Worms were immobilized using 50mM muscimol (Abcam) and hydrogel encapsulation (5). ImageJ was used for image analysis, and it was used to adjust for brightness and contrast for image presentation. All the adjustments were kept identical for direct image comparisons unless otherwise stated. Maximum projections were used for all the confocal images, with the exception of the partial fluorescence recovery photobleaching (FRAP) experiments, which were in single planes. To correct for motion movement of the animal in time-lapse images, acquired image slices were mostly aligned using the Stack registration plugin (7) in ImageJ or manually aligned and then the slices concatenated. Rendering of puncta was performed using Amira visualization software (Thermo Fisher Scientific), where gray values were used to create an isosurface superimposed on a gray-scale representation of the puncta in 3D (see Fig. 4 C). Finally, zoomed insets of images were obtained on ImageJ using the “Zoom in Images and Stacks” plugin developed by Gilles Carpentier.

Quantification of phenotypic penetrance of glycolytic protein clustering and diffuse distribution of synaptic vesicle proteins

Animals were scored as displaying either “punctate” or “diffuse” phenotypes for the fluorophore-tagged glycolytic proteins or synaptic vesicle proteins after specified manipulations. Leica DM500B compound fluorescent microscope was used for the scoring. For hypoxia-induced

conditions, coverslip-induced hypoxia was used as previously described (8) to calculate the percentage of animals displaying PFK-1.1 clusters or diffuse distribution of synaptic vesicle proteins. Statistical analyses were performed with Prism (GraphPad) and p values were calculated using Fisher's exact test.

Examination of subcellular localization of PFK-1.1 and stress granule protein TIAR-1

For heat shock induction, animals on NGM plates seeded with OP50 *Escherichia coli*, were incubated at 37°C for 1hour and were imaged immediately after that as previously described (9, 10). For hypoxia induction, coverslip-induced hypoxia was used as previously described (8). AIY and GABAergic neurons were examined.

Quantifications of subcellular localization of fluorophore-tagged proteins

For still images, the subcellular localization of fluorophore-tagged proteins, including PFK-1.1, were quantified using ImageJ and graphs plotted using Prism (GraphPad). 1) For the distribution of fluorophore-tagged proteins along the neurite, segmented line scans were performed and the graph of fluorescence intensity over distance was plotted. 2) In comparing the total amount of fluorophore-tagged proteins found in the neurite before and after hypoxia, an identical ROI around the neurite was drawn for those two time points. Total fluorescence values were obtained by multiplying the ROI with the mean fluorescence values found in the designated region. Finally, to account for any photobleaching, the raw total fluorescence value was normalized to the percent change of the background.

For time-lapse images, 1) a small ROI encapsulating individual area of the neurite where glycolytic clusters appear was designated in ImageJ and max fluorescence value, or pixel intensity, measured for each time point. The measured max fluorescence value was then plotted against time to show its change over time. 2) A segmented line was drawn through the

neurite and kymograph was generated to show how PFK-1.1 protein localization changes under transient hypoxia using ImageJ. All the images used in the quantification analyses were obtained using identical microscopy settings.

Normalization of max fluorescence

To compare how the max fluorescence changes after repetition of hypoxic and normoxic conditions, we normalized the max fluorescence of individual PFK-1.1 punctum at different time points. First, we identified the PFK-1.1 puncta that repeatedly appeared after the first and second round of hypoxic treatment (10 minutes of hypoxia). Then we measured the max fluorescence of individual punctum and the corresponding region for before hypoxia, after 10 minutes of hypoxia, and after an additional five minutes of normoxia. To account for photobleaching, we used a region that did not have PFK-1.1 puncta formation or localization change to normalize for each max fluorescence value. This value was then further normalized to the starting value or before hypoxic treatment to show the fold changes in max fluorescence through hypoxia and normoxia. *p values* comparing the max fluorescence at different time points were calculated using the Mann-Whitney *U* test.

Neurite diameter measurement

To measure the diameter of the neurite, strains expressing cytosolic mCherry in GABAergic neurons were used. Total of 20 measurements was made by measuring the thickness of the fluorescent signal in the GABAergic neurites. Given the varicosity of the neurite, 10 total measurements were made in the synaptic bouton (mean average of 0.83 μm) and the other 10 measurements were made in the non-bouton areas (mean average of 0.45 μm). Total average was calculated by combining all 20 measurements. We also calculated the neurite diameter from GABAergic electron microscopy images in (11).

PFK-1.1 condensate reversal time measurement

The time (in minutes) it takes for PFK-1.1 in its condensate form to disperse in the cytosol was measured and compared between PFK-1.1 condensates that formed after 10 minutes of transient hypoxia and 40 minutes of prolonged hypoxia. To detect the time for the PFK-1.1 condensate to fully disperse, time-lapse images were acquired from the beginning of the hypoxic treatment to up to 30 minutes of normoxic conditions. A condensate was considered as dispersed in the cytosol when the condensate was no longer distinguishable from the background cytoplasmic signal and loss of the spherical shape.

Supplementary Video Legends

Video S1. PFK-1.1 condensates induced by transient hypoxia reverts back to diffuse localization when the condition is returned to normoxia. Transient hypoxia initiates at time 01:20 (minute:second), and also indicated by the appearance of the green square on the top right corner. Hypoxia is terminated 20 minutes later at 21:20. PFK-1.1 condensates can be seen dispersing after 21:20. See also Fig. 3 E. Scale, 5 μm.

Video S2. **PFK-1.1 condensates repeatedly form and disperse during hypoxia-normoxia cycles.** Two rounds of 10 minutes of transient hypoxia (indicated by the appearance of a green square on the top right corner) interspaced with 5 minutes of normoxia are shown. A small region (white outlined box) of the neurite is zoomed in (2x; yellow outlined box) and the outline of PFK-1.1 localization in the same small region is shown on the bottom left corner. Elapsed time is shown in minute:second. See also Fig. 3 F. Scale, 5 μm.

Video S3. PFK-1.1 condensates undergo fusion. The two PFK-1.1 condensates (in the white outlined box) can be seen fusing and relaxing into a spherical shape. A 2x zoomed inset is shown above. Elapsed time is shown in minute:second on the top left corner. Here, 00:00 is post 8 minutes of transient hypoxia. See also Fig. 4 C. Scale, 2 μm.

Video S4. PFK-1.1 condensates exchange material and undergo fusion. The first PFK-1.1 condensate appear around 12 minutes into hypoxia (elapsed time shown as “minute:second” on the top left corner). Another one appears immediately to the right of it around 15 minutes post hypoxia, and the fluorescence intensity between the two condensates fluctuates until around 32 minutes post hypoxia, which then ends with a fusion event. See also Fig. S5 A. Scale, 2 μm.

Video S5. PFK-1.1 condensates exchange materials. Four PFK-1.1 condensates appear in the white boxed region during transient-hypoxia as indicated by the elapsed time on the top left corner in minute:second. 2x zoomed in inset is shown immediately below. The condensates demonstrate fluctuation in fluorescence intensity, suggesting material exchange between the neighboring condensates. See also Fig. 4 E and F. Scale, 2 μm.

Video S6. PFK-1.1 condensates do not all fuse, but do have fluid-like movements. Elapsed time is shown in minute:second on the top left corner. Here, 00:00 is post 30 minutes of prolonged hypoxia. PFK-1.1 condensates in the white boxed region, instead of fusing, “bounce” of each other. Note that compared to the fusion event (shown in Fig. 4 C and Video S3), which happened after approximately 10 minutes into transient hypoxia, the event recorded here is post 30 minutes of prolonged hypoxia. A 2x zoomed inset is shown at the bottom left. See also Fig. S6 B. Scale, 2 μm.

Video S7. PFK-1.1 clusters asynchronously appear in response to transient hypoxia. Hypoxic condition, which is indicated by the appearance of a green square on the top right, starts at time 00:00 (minute:second). See also Fig. 6A. Scale, 5 μm.

Video S8. PFK-1.1 and ALDO-1 dynamically relocalize into condensates under hypoxia. PFK-1.1::mRuby-3 and ALDO-1::EGFP were co-expressed in GABAergic neuron. Three panels shown, from the left, PFK-1.1 (magenta), ALDO-1 (green), and a merge of the two channels (white). Hypoxic condition, which is indicated by the appearance of a green square on the top right, starts at time 00:00. In the middle of the neurite shown here, there is an appearance of a condensate for PFK-1.1 and ALDO-1 around 10 minutes post-hypoxia, which separates into two condensates by ~23 minutes post-hypoxia. Scale bar, 2um.

Supplementary Figures

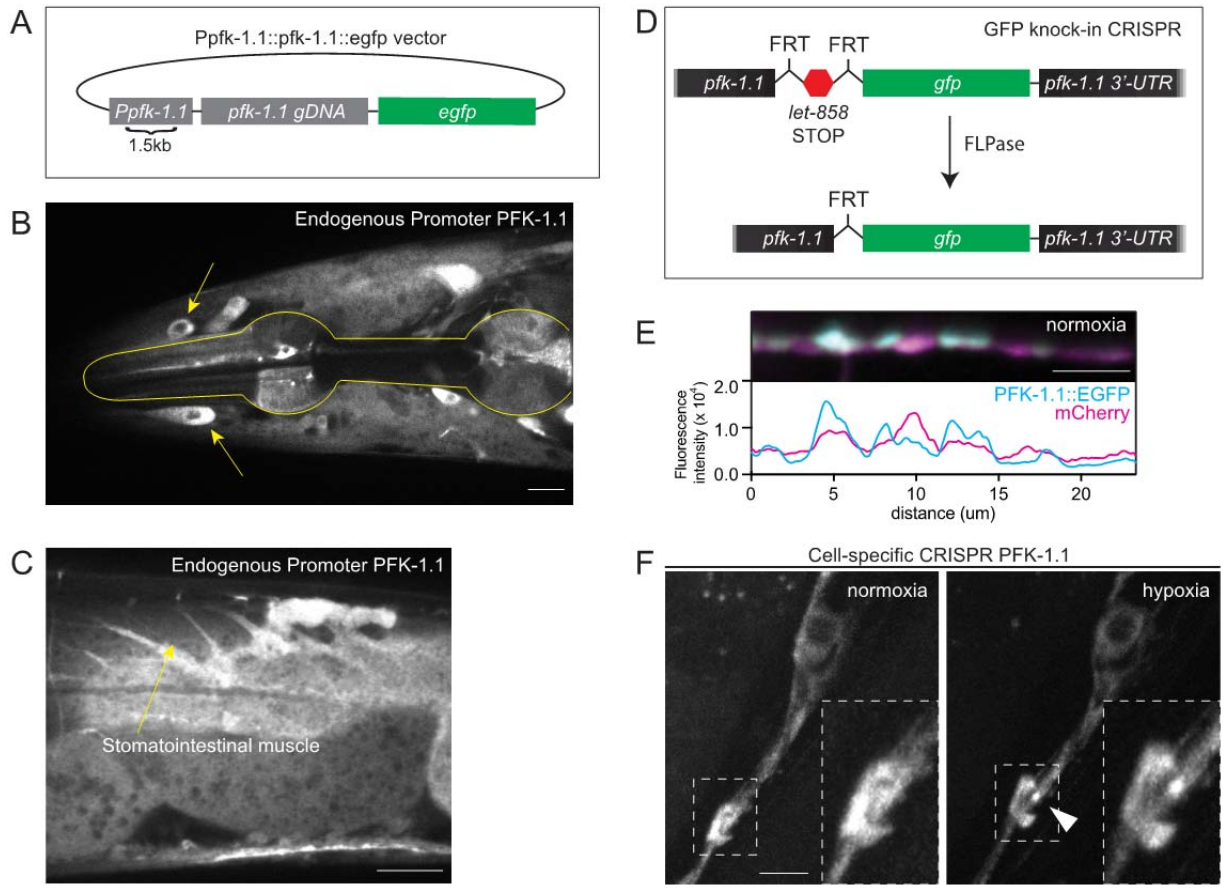

Figure S1. Expression and subcellular localization of PFK-1.1. (**A**) Schematic of the expression vector for PFK-1.1:EGFP driven by its own promoter (Ppfk-1.1:PFK-1.1::EGFP). *Ppfk-1.1* contains 1.5 kilobase (kb) region upstream of the *pfk-1.1* start codon. *pfk-1.1 gDNA* is the genomic sequence of *pfk-1.1* that contains both introns and exons. (**B**) Head of *C. elegans* expressing the *Ppkf-1.1::pfk-1.1::egfp* array. Expression of PFK-1.1 can be seen in the pharyngeal muscle, as outlined, and in other unidentified cells (arrow). Scale, 10 μm. (**C**) Near the tail region of the animal, PFK-1.1 expression is observed in the stomatointestinal muscle.

Scale, 15 μm. (**D**) Schematic of the strategy used for tissue-specific tagging of endogenous PFK-1.1 via conditional CRISPR. (**E**) Cytosolic mCherry (magenta) co-expressed with PFK-1.1 (cyan) in GABAergic neurons to observe the relative distribution of PFK-1.1. Note uneven enrichment of PFK-1.1 through different subcellular neuronal regions even in normoxic conditions. Line scan for PFK-1.1 and mCherry fluorescence level in lower panel. Scale, 5 μm. (**F**) The *unc-47* promoter was used in conditional CRISPR lines to tag the endogenous PFK-1.1 with GFP in a subset of tissues. After 30 minutes of hypoxia, PFK-1.1 clusters can be seen (arrowhead, right panel). Scale, 5 μm.

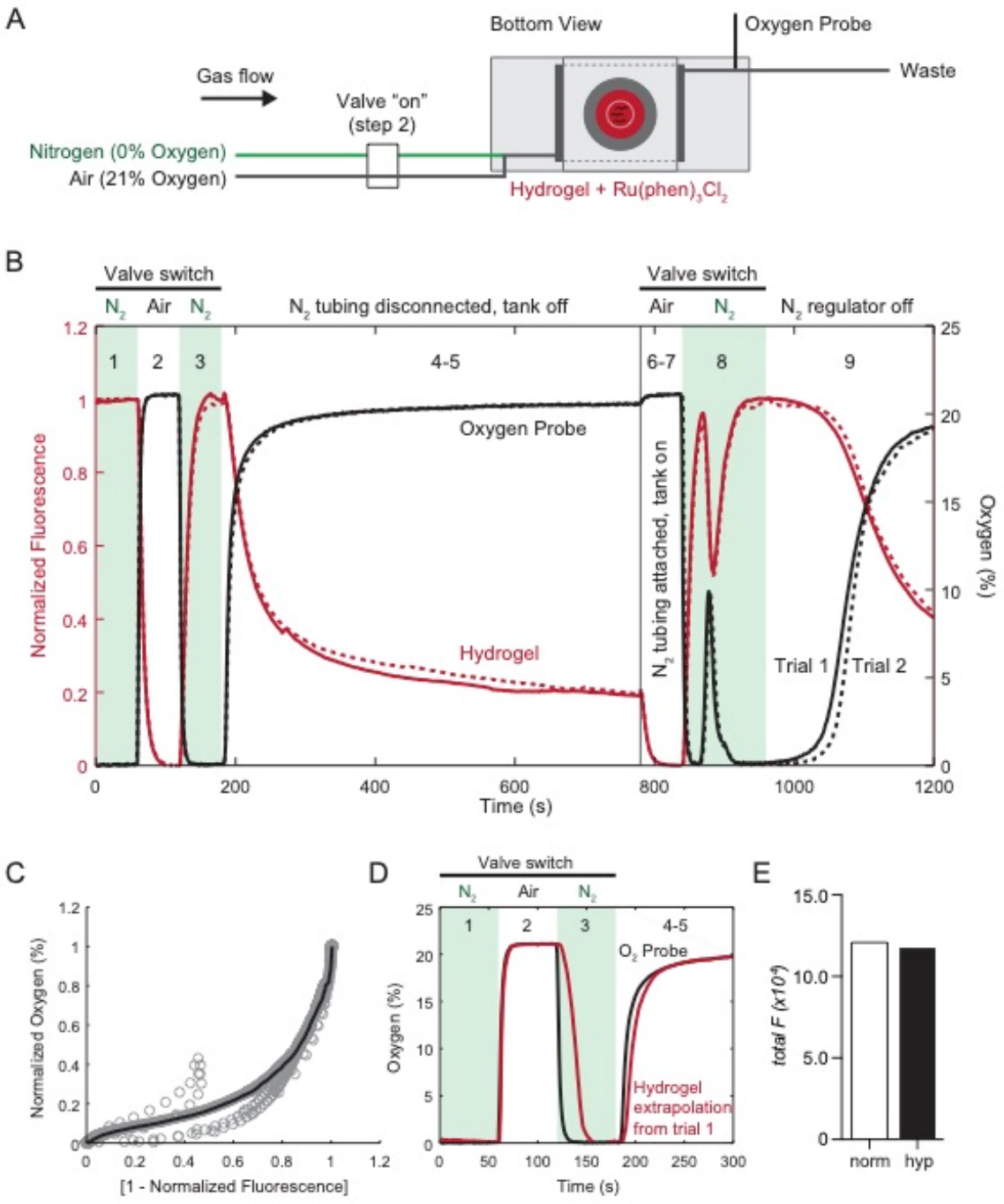

Figure S2. Hybrid microfluidic-hydrogel device and its validation analysis. (**A**) Schematic of hybrid microfluidic-hydrogel device set up for calibration experiments. A pinch valve was used to control flow from compressed nitrogen and air tanks. When the valve was powered "on" using a custom Arduino microcontroller, air flowed through the chamber to the hydrogel and outlet

(shown), in which oxygen concentration levels were continuously monitored using an oxygen probe. Synchronous changes in $Ru(phen)_3Cl_2$ fluorescence were monitored in the hydrogel by epifluorescence microscopy. When the valve was not powered, nitrogen flowed through the chamber (hypoxia) and outlet. (**B**) Line plot of synchronized oxygen probe and epifluorescence microscopy measurements (of $Ru(phen)_3Cl_2$ fluorescence) during a semi-automated sequence of valve switches. First, three valve-controlled switches from (1) nitrogen to (2) air to (3) nitrogen were delivered to observe steady-state minimum and maximum fluorescence intensities, followed by (4) manually turning off the nitrogen tank and (5) immediately disconnecting the nitrogen inlet tubing from the tank for 10 minutes. Next, a valve switch allowed (6) air flow to enter the device to determine shifts in baseline fluorescence. During this time, the nitrogen tubing was (7) re-attached and the tank was turned back on. Another valve switch (8) was used to restore low oxygen levels, yielding a short increase in oxygen likely due to air entering the previously disconnected nitrogen tubing. Finally, to compare differences in switching delays, the nitrogen regulator was (9) turned off and immediately back on after completing the 1200 second acquisition. The exact sequence was executed for a second trial (dashed line) and shown. (**C**) Scatter plot of all normalized oxygen concentrations larger than normalized fluorescence values versus [1 – normalized fluorescence]. Trend line represents the median values of binned oxygen concentration values, with linear interpolation between bins. (**D**) Estimated oxygen concentration in the hydrogel (using the calibration curve in **C**) compared with measured oxygen concentration in the gas channel for the first 300 s in B. (**E**) Total fluorescence of PFK-1.1 in Fig. 2 D neurite for normoxic condition (white box, “norm”) and transiently hypoxic conditions (black box, “hyp”). Note that there are no significant changes in the total levels of neurite fluorescence between the two conditions.

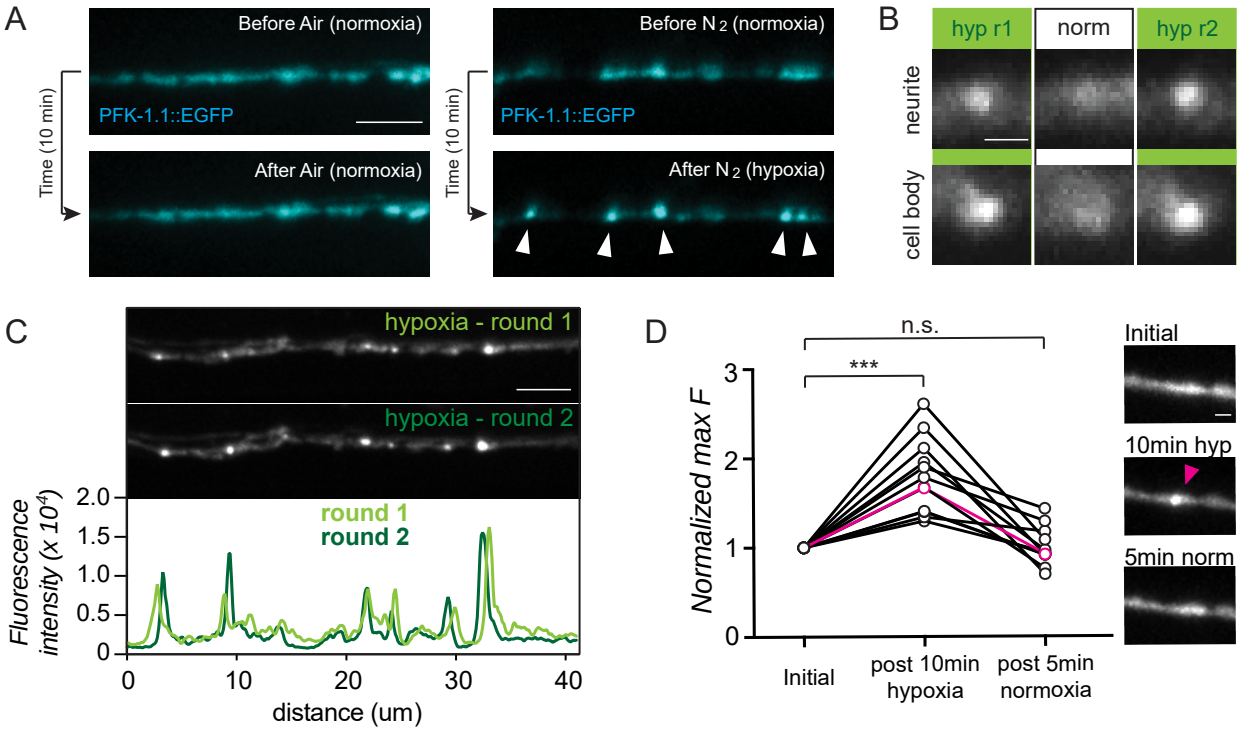

Figure S3. Reversibility of PFK-1.1 condensates. (**A**) PFK-1.1::EGFP before gas treatment (top panels) and after exposure to gas treatment for 10 minutes (bottom panels) with either normal air (left panels) or nitrogen gas (right panels). PFK-1.1 condensates (arrowheads) form specifically in response to transient hypoxic conditions. Scale, 5 μm. (**B**) PFK-1.1 condensates repeatedly appear in both the neurites (top panels) and cell bodies (bottom panels) of neurons through two rounds (r1 and r2) of normoxia ("norm") and transient hypoxia ("hyp") cycles. Scale, 1 μm. (**C**) PFK-1.1 localization after the first round of transient hypoxia (top panel) and the second round of transient hypoxia (middle panel). Note how PFK-1.1 condensates reappear at similar locations (this is another example of an additional neurite, as in Fig. 2 F, G). In lower panel, corresponding line scan for each round of transient hypoxia are shown: first round (light green) and second round (dark green). Scale, 5 μm. (**D**) Calculation of the normalized maximum fluorescence of twelve different neurite regions where PFK-1.1 condensates appear after 10 minutes of transient hypoxia and disperse after an additional five minutes of normoxia. Values

were normalized to the initial maximum fluorescence value prior to transient hypoxia treatment. The normalized maximum fluorescence values showed significant increases by 1.79 +/- 0.12 fold (normalized mean fold +/- SEM; N=12 condensates) after transient hypoxia, and return to the basal level of 1.00 +/- 0.06 fold (normalized mean fold +/- SEM; N=12 condensates) after five minutes of normoxia. Right panels: image of the neurite prior to transient hypoxia treatment (top, labeled “Initial”), after condensate formation upon ten minutes of transient hypoxia (middle, labeled “10 min hyp”, with condensate pointed out by arrowhead), and upon five minutes of normoxia (lower, labeled “5 min norm”) corresponding to a representative condensate (in magenta) on the graph. Scale, 1 μm.

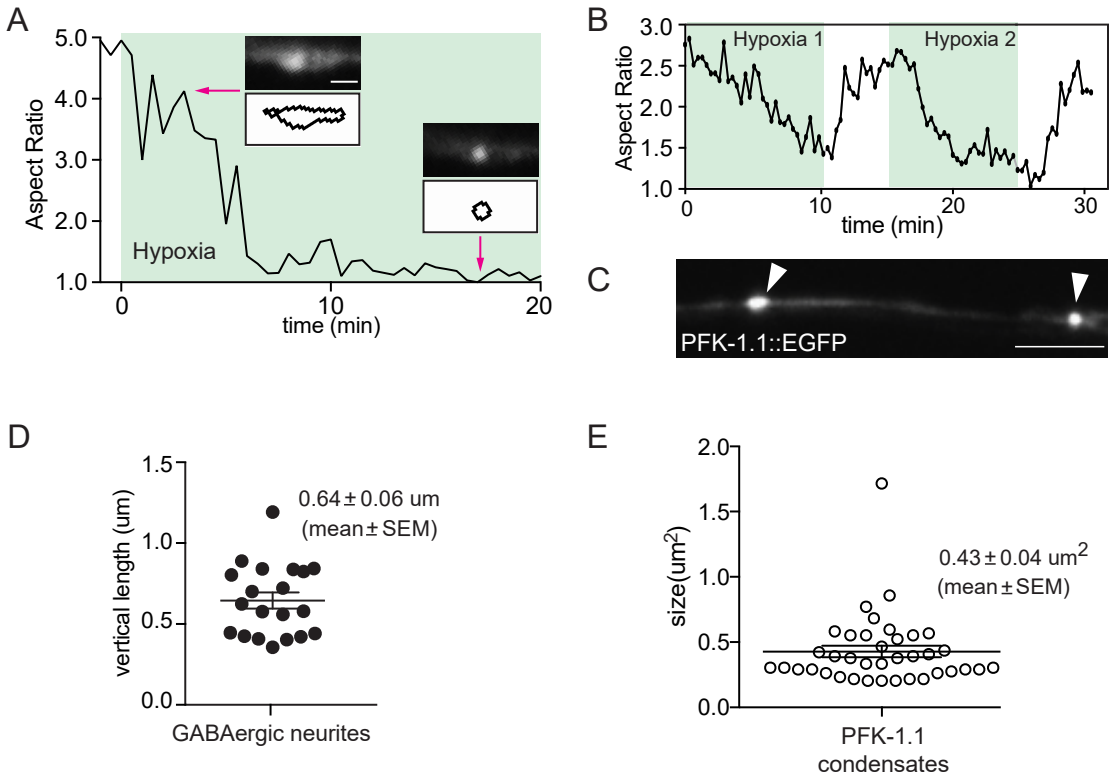

Figure S4. Aspect ratio of PFK-1.1 condensates. (**A**) Changes in the aspect ratio of PFK-1.1 for a given condensate over time. Once transient hypoxia was initiated (green region), the PFK-1.1 coalesced into a spherical structure. Two representative images (left: 3 minutes post-onset of transient hypoxia; right: 17.5 minutes post-onset of transient hypoxia) and corresponding outline of their morphology (white outlined boxes below) used to calculate the aspect ratio. Scale, 2 μm. (**B**) Changes in the aspect ratio of the PFK-1.1 condensates corresponding to Fig. 3 F over time. (**C**) Bigger PFK-1.1 condensates (left arrowhead) look like spherocylinders, as compared to smaller condensates (right arrowhead), which are spherical, suggesting that neurite space may constrain the shape of the fluid condensates. Scale, 5 μm. (**D**) We measured the diameter of GABAergic neurites, as visualized with cytoplasmic mCherry (also measured from electron micrographs, data not shown). Mean vertical length was 0.64 μm (N=20 neurite regions), which would only allow a perfect sphere with a volume of 0.14 μm^3 to fit. (**E**) Measurement of PFK-1.1 condensate size shows an average area of 0.43 +/- 0.04 μm^2 (mean +/- SEM; N=38 condensates) Assuming radial symmetry, its volume would be 0.21 μm^3.

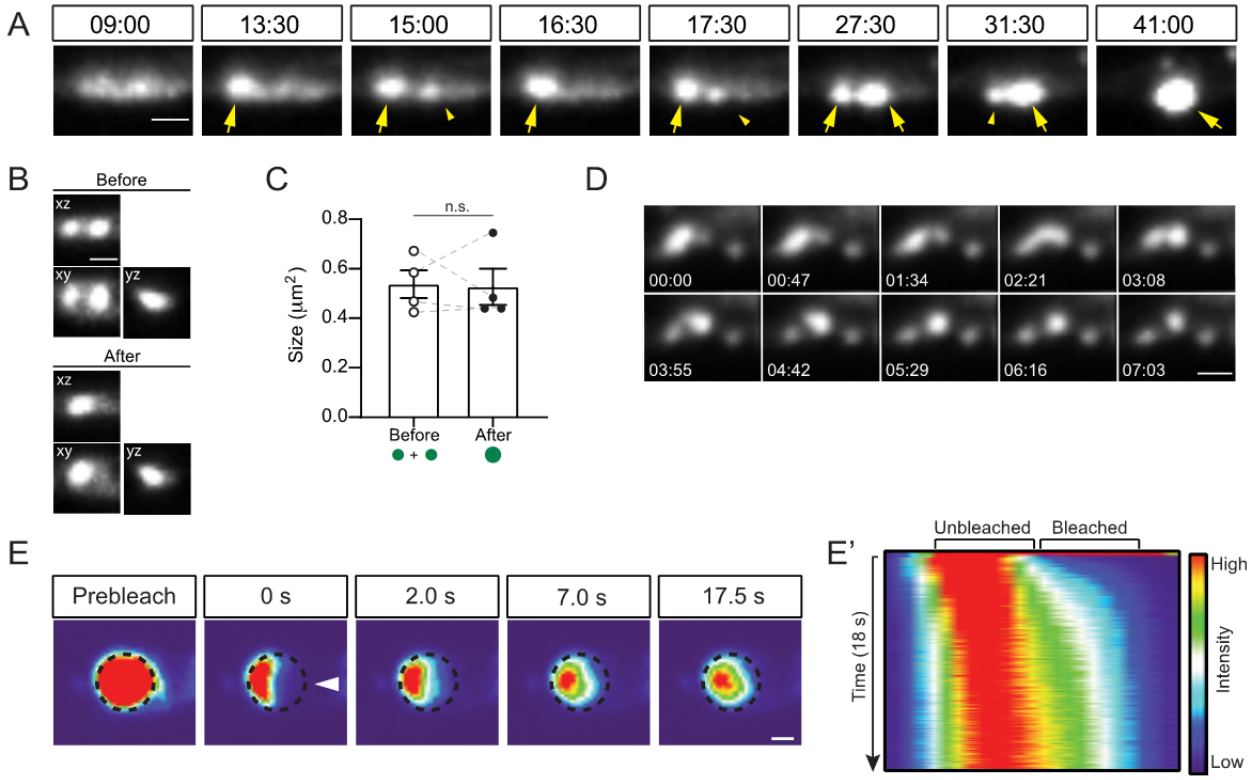

Figure S5. Liquid-like properties of PFK-1.1 condensates. (**A**) Fluid dynamics of two neighboring PFK-1.1 condensates (yellow arrows) upon transient hypoxia (minutes:seconds after induction of transient hypoxia specified on top of the images). The first PFK-1.1 condensate appears in the second montage (13:30) and the second condensate appears soon after (third montage, 15:00). The fluorescence intensity between the two condensates fluctuates until around 32 minutes post hypoxia, which then ends with a fusion event between the two. See also Video S5. Scale, 1 µm. (**B**) Max projection from three different planes (xy, yz, and xz) before fusion and after fusion of Fig. 4 C from three projections (xz, xy and yz) demonstrating fusion. (**C**) Quantification of four separate fusion events (each connected by dotted gray lines). When the total area of PFK-1.1 condensates is measured before fusion (open circles), and after fusion (black circle), no significant difference is observed. (**D**) Additional timeframes for Fig. 4 D. Elapsed time from the beginning of the imaging session is indicated for each image in

minutes:seconds. Scale, 1 μm. (**E-E'**) Fluorescence recovery after photobleaching of a PFK-1.1 condensate in the cell body of a neuron also shows similar recovery dynamics to those observed in the neurites (compare with Fig. 5 A). PFK-1.1::EGFP condensate initial shape outlined with dashed circle, and partial area bleached highlighted with arrowhead in second panel. Scale, 1 μm. In C', kymograph of the partially bleached condensate and recovery dynamics.

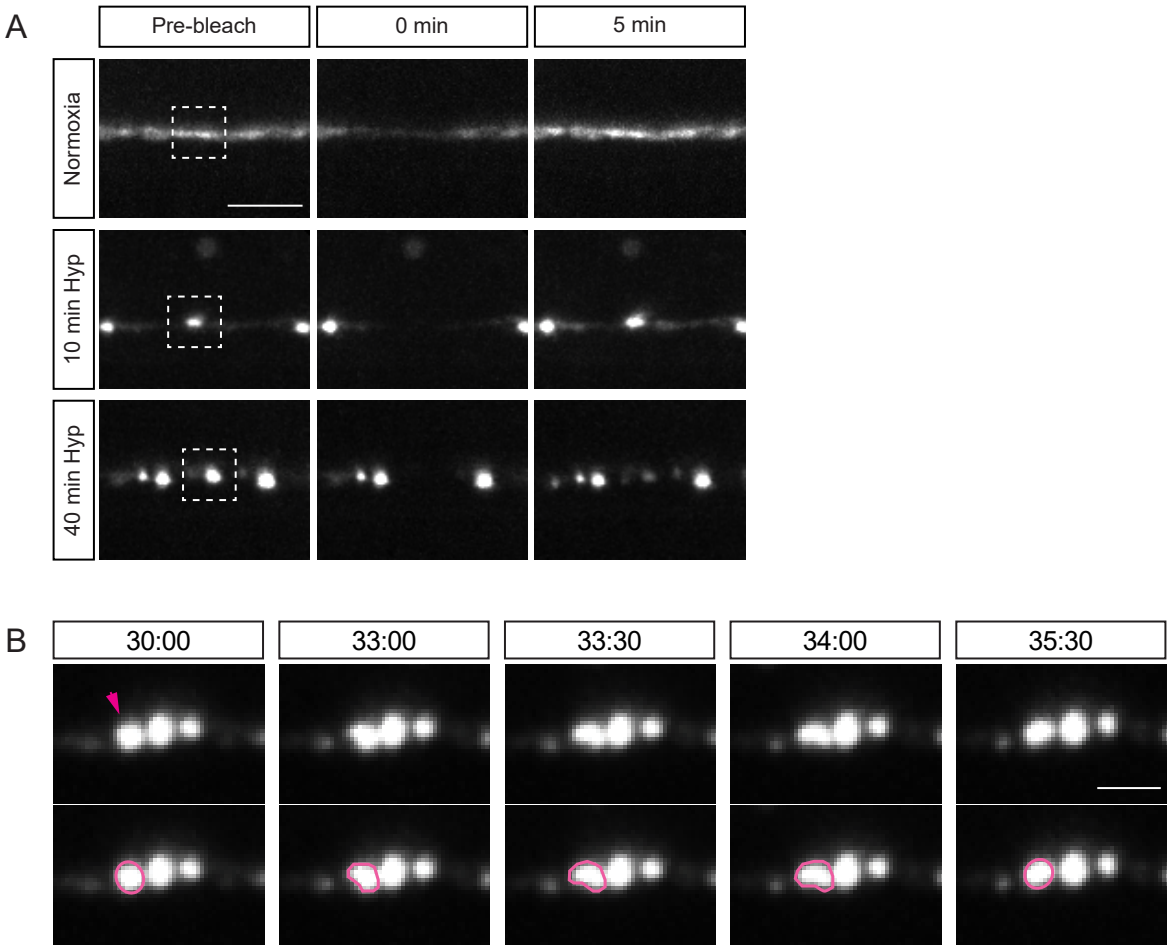

Figure S6. Changes in PFK-1.1 condensate properties. (**A**) Complete photobleaching of PFK-1.1 condensates, and fluorescence recovery. Dashed box indicates the photo-bleached area. Before photobleaching (Pre-bleach), at the time of photobleaching (0 min) and post 5 minutes of photobleaching are shown for PFK-1.1 under three conditions: normoxia, after 10 minutes of hypoxia and 40 minutes of hypoxia. We note that besides the proposed changes in the material properties of the condensates, there could also be a corresponding deeper quench of the cytoplasmic PFK-1.1 material, resulting in a concomitant lower protein concentration in the dilute phase during the hardening of the condensates from prolongued hypoxia. Scale, 5 µm. (**B**) A PFK-1.1 condensate displays fluid motions (magenta arrowhead and outline in lower panels) as it bounces away from its closely neighboring condensates. Time elapsed since the

start of transient hypoxia is indicated above in minutes:seconds. See also Video S6. Scale, 2 µm.

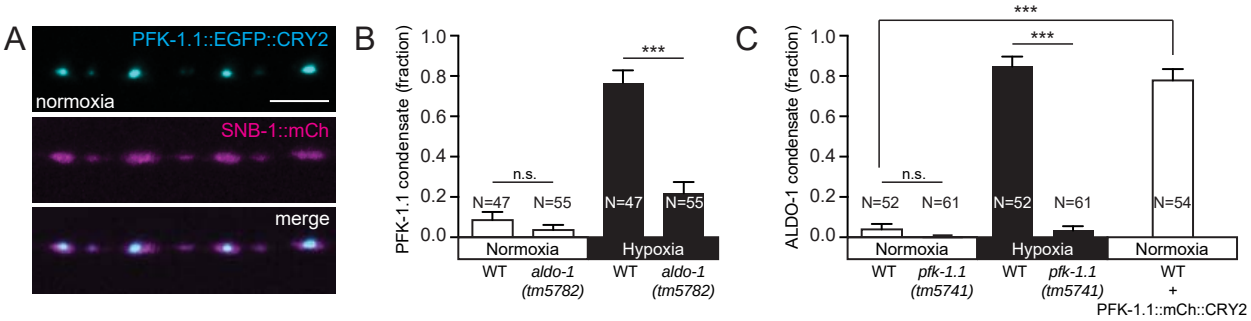

Figure S7. PFK-1.1 and ALDO-1 condensates

(**A**) PFK-1.1::EGFP::CRY2 (cyan) forms clusters near synapses (as visualized with SNB-1/synaptobrevin (magenta) in GABAergic neuron) even in normoxic conditions, indicating the ability of CRY2 to promote condensate formation. Scale, 5 µm. (**B**) Fraction of animals that display PFK-1.1::EGFP condensates for in wild-type (WT) or *aldo-1 (tm5782)* mutant backgrounds (from Fig. 7 F). (**C**) Fraction of animals that display ALDO-1::EGFP condensates in in wild-type (WT) or *pfk-1.1 (tm5741)* mutant background (from Fig. 7 G) or ALDO-1::EGFP co-expressed with PFK-1.1::mCh::CRY2 (from Fig. 7 H). N indicates the number of animals scored. Error bars denote SEM. *, $p < 0.05$. **, $p < 0.01$. ***, $p < 0.001$ between indicated group.

Supporting References

1. Dickinson, D.J., A.M. Pani, J.K. Heppert, C.D. Higgins, and B. Goldstein. 2015. Streamlined Genome Engineering with a Self-Excising Drug Selection Cassette. *Genetics*. 200:1035–1049.

2. Schwartz, M.L., and E.M. Jorgensen. 2016. SapTrap, a Toolkit for High-Throughput CRISPR/Cas9 Gene Modification in Caenorhabditis elegans. *Genetics*. 202:1277–1288.

3. Mello, C., and A. Fire. 1995. DNA transformation. *Methods Cell Biol*. 48:451–82.

4. Lagoy, R.C., and D.R. Albrecht. 2015. Microfluidic Devices for Behavioral Analysis, Microscopy, and Neuronal Imaging in Caenorhabditis elegans. *Methods Mol Biol*. 1327:159–79.

5. Burnett, K., E. Edsinger, and D.R. Albrecht. 2018. Rapid and gentle hydrogel encapsulation of living organisms enables long-term microscopy over multiple hours. *Commun. Biol.* 1:73.

6. Powell-Coffman, J.A. 2010. Hypoxia signaling and resistance in C. elegans. *Trends Endocrinol. Metab. TEM*. 21:435–440.

7. Thévenaz, P., U.E. Ruttimann, and M. Unser. 1998. A pyramid approach to subpixel registration based on intensity. *IEEE Trans. Image Process. Publ. IEEE Signal Process. Soc.* 7:27–41.

8. Jang, S., J.C. Nelson, E.G. Bend, L. Rodriguez-Laureano, F.G. Tueros, L. Cartagenova, K. Underwood, E.M. Jorgensen, and D.A. Colon-Ramos. 2016. Glycolytic Enzymes Localize to Synapses under Energy Stress to Support Synaptic Function. *Neuron*. 90:278–91.

9. Huelgas-Morales, G., C.G. Silva-García, L.S. Salinas, D. Greenstein, and R.E. Navarro. 2016. The Stress Granule RNA-Binding Protein TIAR-1 Protects Female Germ Cells from Heat Shock in Caenorhabditis elegans. *G3 Bethesda Md*. 6:1031–1047.

10. Sun, Y., P. Yang, Y. Zhang, X. Bao, J. Li, W. Hou, X. Yao, J. Han, and H. Zhang. 2011. A genome-wide RNAi screen identifies genes regulating the formation of P bodies in C. elegans and their functions in NMD and RNAi. *Protein Cell*. 2:918–939.

11. Xuan, Z., L. Manning, J. Nelson, J.E. Richmond, D.A. Colon-Ramos, K. Shen, and P.T. Kurshan. 2017. Clarinet (CLA-1), a novel active zone protein required for synaptic vesicle clustering and release. *Elife*. 6.